



Human parvovirus B19 causes cell cycle arrest of human erythroid progenitors via deregulation of the E2F family of transcription factors

Zhihong Wan,¹ Ning Zhi,¹ Susan Wong,¹ Keyvan Keyvanfar,¹ Delong Liu,² Nalini Raghavachari,³ Peter J. Munson,² Su Su,¹ Daniela Malide,⁴ Sachiko Kajigaya,¹ and Neal S. Young¹

¹Hematology Branch, National Heart, Lung, and Blood Institute, NIH, Bethesda, Maryland, USA. ²Center for Information Technology, NIH, Bethesda, Maryland, USA. ³Gene Expression Core Facility and ⁴Light Microscopy Core Facility, National Heart, Lung, and Blood Institute, NIH, Bethesda, Maryland, USA.

Human parvovirus B19 (B19V) is the only human pathogenic parvovirus. It causes a wide spectrum of human diseases, including fifth disease (erythema infectiosum) in children and pure red cell aplasia in immunocompromised patients. B19V is highly erythrotropic and preferentially replicates in erythroid progenitor cells (EPCs). Current understanding of how B19V interacts with cellular factors to regulate disease progression is limited, due to a lack of permissive cell lines and animal models. Here, we employed a recently developed primary human CD36⁺ EPC culture system that is highly permissive for B19V infection to identify cellular factors that lead to cell cycle arrest after B19V infection. We found that B19V exploited the E2F family of transcription factors by downregulating activating E2Fs (E2F1 to E2F3a) and upregulating repressive E2Fs (E2F4 to E2F8) in the primary CD36⁺ EPCs. B19V nonstructural protein 1 (NS1) was a key viral factor responsible for altering E2F1–E2F5 expression, but not E2F6–E2F8 expression. Interaction between NS1 and E2F4 or E2F5 enhanced the nuclear import of these repressive E2Fs and induced stable G₂ arrest. NS1-induced G₂ arrest was independent of p53 activation and increased viral replication. Downstream E2F4/E2F5 targets, which are potentially involved in the progression from G₂ into M phase and erythroid differentiation, were identified by microarray analysis. These findings provide new insight into the molecular pathogenesis of B19V in highly permissive erythroid progenitors.

Introduction

Parvovirus B19 (B19V), a member of the *Erythrovirus* genus of the Parvoviridae family, is a widespread human pathogen. B19V is the causative agent of a variety of human diseases: fifth disease (erythema infectiosum) in children, hydrops fetalis in pregnant women, and transient aplastic crisis in patients with underlying chronic hemolytic anemia or pure red cell aplasia in immunocompromised patients (1). Some evidence also suggests that B19V is associated with autoimmune diseases, including arthritis (2, 3), vasculitis (4), and autoimmune neutropenia (5). The molecular pathogenesis of B19V infection is largely unknown, since there are no fully permissive cell lines, due to the virus's extreme tropism for human erythroid progenitor cells (EPCs), and no experimental animals susceptible to B19V infection. Previous studies have suggested that cell surface membrane receptors (6, 7), as well as cellular factors that are essential for viral DNA replication (8) and RNA maturation (9), are related to the restricted permissiveness for viral propagation.

B19V has a small (22 nm), nonenveloped, icosahedral capsid with a single-stranded DNA genome that encodes nonstructural protein 1 (NS1), two capsid proteins (VP1 and VP2), and two smaller proteins (7.5 kDa and 11 kDa). The major and minor capsid proteins, VP2 and VP1, are identical except for 227 amino acids at the VP1 amino-terminal end known as the VP1 unique

region (VP1u) (10). A conserved phospholipase A₂-like (PLA₂-like) motif (HDXXY) is present in the VP1u region in members of the Parvoviridae family (11), including B19V (12). A point mutation in the PLA₂ motif significantly attenuates the infectivity of B19V, suggesting a critical role for PLA₂ in the B19V life cycle (13). The 7.5-kDa and 11-kDa proteins encoded by abundant small mRNAs of B19V are unique among the parvoviruses characterized to date. Recently, Chen et al. reported that the 11-kDa protein is a significant inducer of apoptosis in erythroid progenitors (14). NS1 is cytotoxic and plays a crucial role in B19V pathogenesis. NS1 is a multifunctional protein that is involved in regulation of viral p6 promoter activity, DNA replication (15–17), cell cycle arrest in G₁ and G₂ phases in erythroid lineage cells (18, 19), and initiation of apoptosis (20). NS1 also functions as a transcriptional transactivator, regulating a variety of viral and cellular genes, such as *TNFA* (21) and *p21^{WAF1/CIP1}* (22). NS1 contains a nucleoside triphosphate-binding motif relating to NS1 cytotoxicity (23). However, the molecular mechanism by which NS1 mediates cellular changes is not fully understood.

The E2F family of transcription factors, which consists of 8 members (E2F1–E2F8) (24), plays a central role in regulating cell cycle progression, DNA replication, DNA repair, differentiation, and apoptosis. E2F family members are divided into 3 subgroups, based on their transcriptional properties and their interaction potentials with pocket proteins (p130, p107, and retinoblastoma protein [pRb]) (25). E2F1, E2F2, and E2F3a are potent transcriptional activators and facilitate cell cycle progres-

Authorship note: Zhihong Wan and Ning Zhi contributed equally to this work.

Conflict of interest: The authors have declared that no conflict of interest exists.

Citation for this article: *J Clin Invest.* 2010;120(10):3530–3544. doi:10.1172/JCI41805.



sion from G₁ to S phase. E2F4 and E2F5 are thought to act primarily as transcriptional repressors when bound to p130 during the G₀/G₁ phase of the cell cycle. Previous studies have suggested that E2F4 and E2F5 also play essential roles in pocket protein-mediated G₁ or G₂ control (26, 27). E2F6, E2F7, and E2F8 act as pocket protein-independent transcriptional repressors, due to lack of transactivation and pocket protein-binding domains. Further, the surprising complexity of E2F-dependent transcriptional control has been reported, suggesting that E2F-mediated transcriptional activation and repression mechanistically overlap (28). Nuclear translocation of E2F4 and E2F5 is dependent on pocket and DP protein binding because both of them lack a nuclear localization signal (NLS). In addition, the phosphorylation status of pocket and DP proteins, as well as E2F4/E2F5, affect their associations (29, 30). Certain viruses with DNA genomes specifically target the E2F/pRb pathway and perturb cell cycle progression, presumably creating a more hospitable environment for viral replication. For DNA tumor viruses, the interaction of herpes simplex virus DE ICP8 (delayed-early single-strand DNA-binding protein) (31), Epstein-Barr virus latent membrane protein 1 (LMP1) (32), human papillomavirus E7 (33), or adenovirus E1A protein (34) with E2Fs or pocket proteins usually has a positive impact on cell cycle progression, leading to tumorigenesis. In contrast, adenovirus-associated virus Rep78 protein displays an oncosuppressive property by associating with the E2F1 protein and stabilizing the pRb-E2F1 complex so as to decrease E2F1 activity (35).

Recently, we developed a cell culture system that allows differentiation and expansion of CD34⁺ HSCs into CD36⁺ EPCs, which are highly permissive to B19V infection and replication, providing a cellular system that mimics *in vivo* infection of this pathogenic human virus (36). B19V infection results in a rapid arrest of cell proliferation in the primary CD36⁺ EPCs (36). Given the important roles of E2Fs in cell proliferation and cell cycle progression, we investigated effects of E2F transcription factors on B19V-induced arrest of cell proliferation and cell cycling in CD36⁺ EPCs. We found marked changes in E2F transcription factors upon B19V infection and elucidated a unique interaction between B19V NS1 and E2F4 or E2F5, which enhances the nuclear import of these repressive E2Fs from cytoplasm to nucleus and induces stable G₂ arrest by target gene repression.

Results

B19V NS1 protein induces stable G₂ arrest in CD36⁺ EPCs. To address whether B19V infection arrested cell cycle progression of primary CD36⁺ EPCs, we measured cumulative proliferation, BrdU incorporation, and DNA content in these cells following B19V infection. B19V infection caused marked inhibition of CD36⁺ EPC proliferation, with almost static cell numbers over the time course, while the number of mock-infected cells rose approximately 17-fold by day 4 (Figure 1A and Supplemental Table 1; supplemental material available online with this article; doi:10.1172/JCI41805DS1). A time-dependent increase in dead cells was observed — 8%, 14%, 19%, and 23% at 24, 48, 72, and 96 hours postinfection (hpi) — in B19V-infected cells, respectively, but the level was similar (ranging between 3% and 5%) over the experimental time course in mock-infected cells. Consistently, B19V-infected cells exhibited less cellular DNA replication than did mock-infected cells, as indicated by a decrease in BrdU-positive cells in a time-dependent manner: 42%, 26%, and 15% at 24, 48, and 72 hpi, respectively. In contrast, no obvious change

was found in a control population (Figure 1B and Supplemental Table 2). Further, B19V infection led to a time-dependent accumulation of cells in the G₂ phase (25%, 32%, and 42% at 12, 24, and 48 hpi, respectively), whereas no change was observed after mock infection (Figure 1C and Supplemental Table 3).

Since B19V NS1 is known to be cytotoxic and involved in the pathogenesis of B19V infection, NS1 effects on the cell cycle were assessed using NS1-transduced CD36⁺ EPCs. In order to optimize experimental conditions for NS1 expression, we first performed a titration of NS1 lentivirus to determine the correlation between MOI and infectivity by immunofluorescence (IF) analysis using anti-Flag (NS1) antibody. The result revealed that approximately 80% of cells were positive for NS1 when cells were inoculated with NS1 lentivirus at an MOI of 4 or 8 (Supplemental Figure 1A). To avoid overexpression of NS1 in the transduced cells, we conducted real-time RT-PCR to compare the transcription level of NS1 in NS1-transduced and B19V-infected cells. As shown in Supplemental Figure 1B, when NS1 lentivirus was used at an MOI of 4, the NS1 transcription level was similar to that after B19V infection. Based on the results of IF and real-time RT-PCR analyses, we decided to use NS1 lentivirus at an MOI of 4 in our experiments. Similar to B19V infection, NS1 transduction dramatically suppressed cell proliferation, compared with control transduction (empty lentivirus), in which approximately 13-fold elevation was observed by day 4 (Figure 1D and Supplemental Table 1). The ratio of dead cells in NS1-transduced cells was gradually increased to 35% by day 4 (slightly higher than in B19V-infected cells), while the ratio in control cells was much lower (4%–13%) over the time course. These results indicate that the cell death induced by both B19V infection and NS1 transduction also contributes to the anti-proliferative effect, which is likely due to apoptosis.

In comparison with control transduction, NS1 transduction resulted in decreased BrdU incorporation, 34% (NS1) versus 48% (control) at 24 hours posttransduction (hpt), and levels remained essentially the same thereafter (Figure 1E and Supplemental Table 2). This was different from the time-dependent decrease observed in B19V infection and may have been due to lack of secondary infection in NS1-transduced cells. NS1 transduction caused time-dependent accumulation of cells in the G₂ phase: 14%, 42%, and 47% at 12, 24, and 48 hpt, respectively, compared with 10%, 12%, and 8.6% in control samples (Figure 1F and Supplemental Table 3). Overall, these results demonstrate that NS1 impairs cell cycle progression of CD36⁺ EPCs by inducing stable G₂ arrest.

B19V NS1 protein deregulates the E2F family of transcription factors in CD36⁺ EPCs. Given the important role of E2Fs in cell proliferation and cell cycle control, we investigated whether B19V infection of CD36⁺ EPCs altered expression levels of E2F transcription factors. B19V infection caused an obvious reduction in protein levels of activating E2Fs (E2F1, E2F2, and E2F3a) but robust elevation of repressive E2Fs (E2F4, E2F5, E2F6, E2F7, and E2F8) at both 24 and 48 hpi, compared with mock infection (Figure 2A). For E2F4, B19V infection markedly induced its phosphorylated form (upper bands in Figure 2A and Supplemental Figure 2), which coincided with reduction of the unphosphorylated form ubiquitously expressed in uninfected cells. In B19V-infected cells, E2F4, E2F7, and E2F8 exhibited time-dependent increases in the time course tested, while no obvious changes were observed in E2F5 and E2F6.

NS1 transduction of CD36⁺ EPCs almost completely suppressed E2F1 and E2F2 but only moderately suppressed E2F3a, which was accompanied by simultaneous increases in E2F4 (both

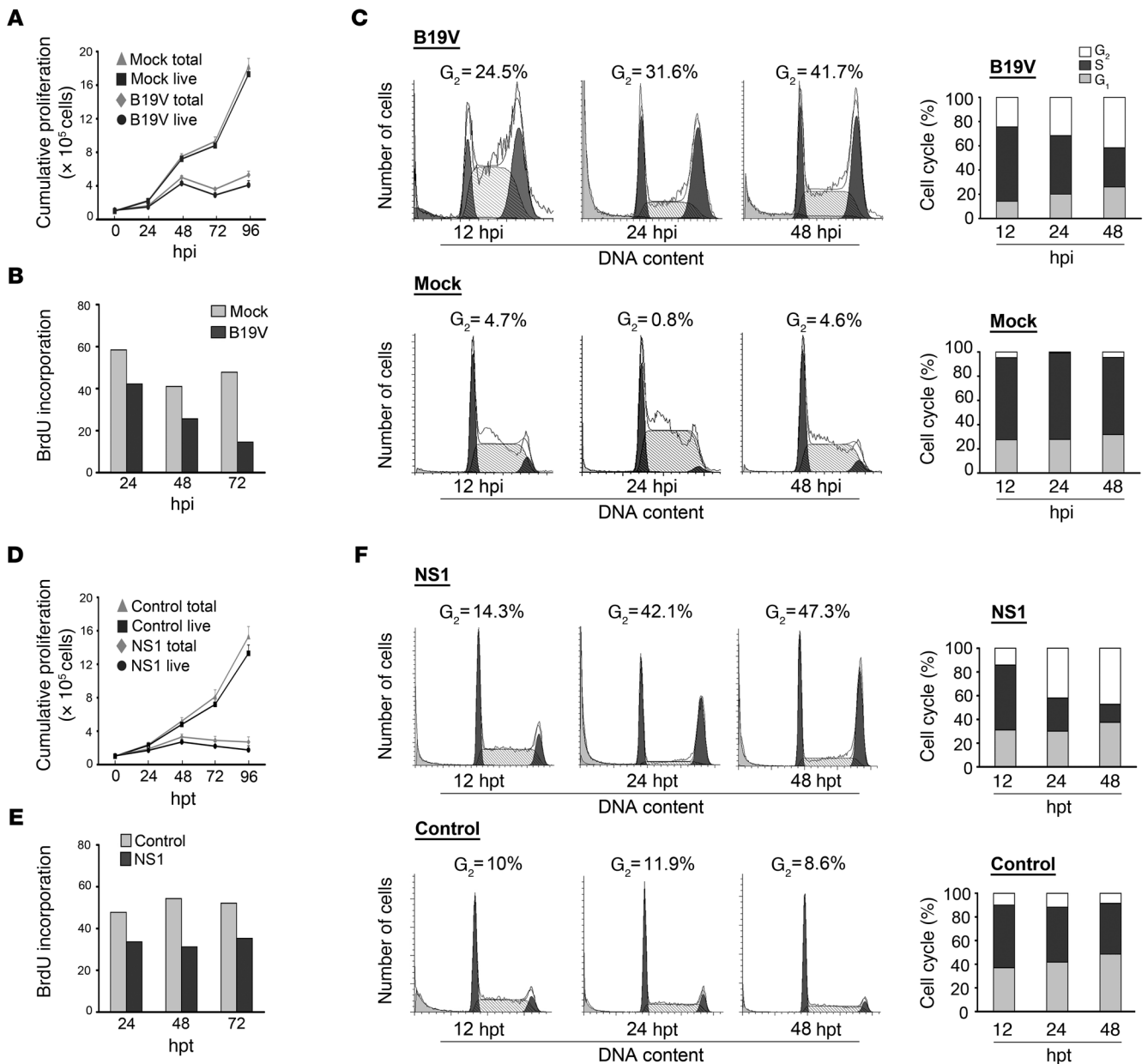


Figure 1 B19V NS1 protein induces stable G₂ arrest in primary CD36⁺ EPCs. CD36⁺ EPCs were B19V- or mock-infected (A–C) or transduced with NS1 or control lentivirus (D–F), followed by harvests at the indicated time points. (A and D) Cumulative proliferation was measured by counting live or dead cells in triplicate using the trypan blue exclusion method, and results are indicated as total and live cell numbers. Data are shown as mean ± SD of 3 independent experiments. (B and E) BrdU incorporation was analyzed by flow cytometry, and percentages of cells stained at the indicated time points are presented. (C and F) Cell cycle analysis was carried out by staining for DNA content, and percentages of cells in different cell cycle phases at indicated time points are presented on the right. Similar results were obtained in duplicate experiments.

phosphorylated and unphosphorylated forms) and E2F5 in CD36⁺ EPCs (Figure 2A). NS1 alone was unable to aggressively reduce E2F3a and failed to efficiently induce phosphorylation of E2F4, results that are in contrast to those after B19V infection. Increases in E2F6, E2F7, and E2F8 were detected in B19V-infected cells but not in NS1-transduced cells, implying roles for other viral elements in the induction of these repressive E2Fs. Collectively, our results suggest that B19V infection deregulates E2F transcription factors in CD36⁺ EPCs, partially due to NS1 expression.

We next sought to identify E2F target genes whose expression was associated with NS1-induced G₂ arrest in CD36⁺ EPCs by performing microarray analysis. In comparison with control transduction, a total of 1,045 genes demonstrated at least a 1.5-fold differential expression when we adopted a false discovery rate (FDR) of 10% (Benjamini-Hochberg procedure) in NS1-transduced cells. A complete gene list with symbols, probe set IDs, accession numbers, and functional descriptions is provided in Supplemental Table 7. Genes with an absolute fold change of 1.5 or more at each corresponding

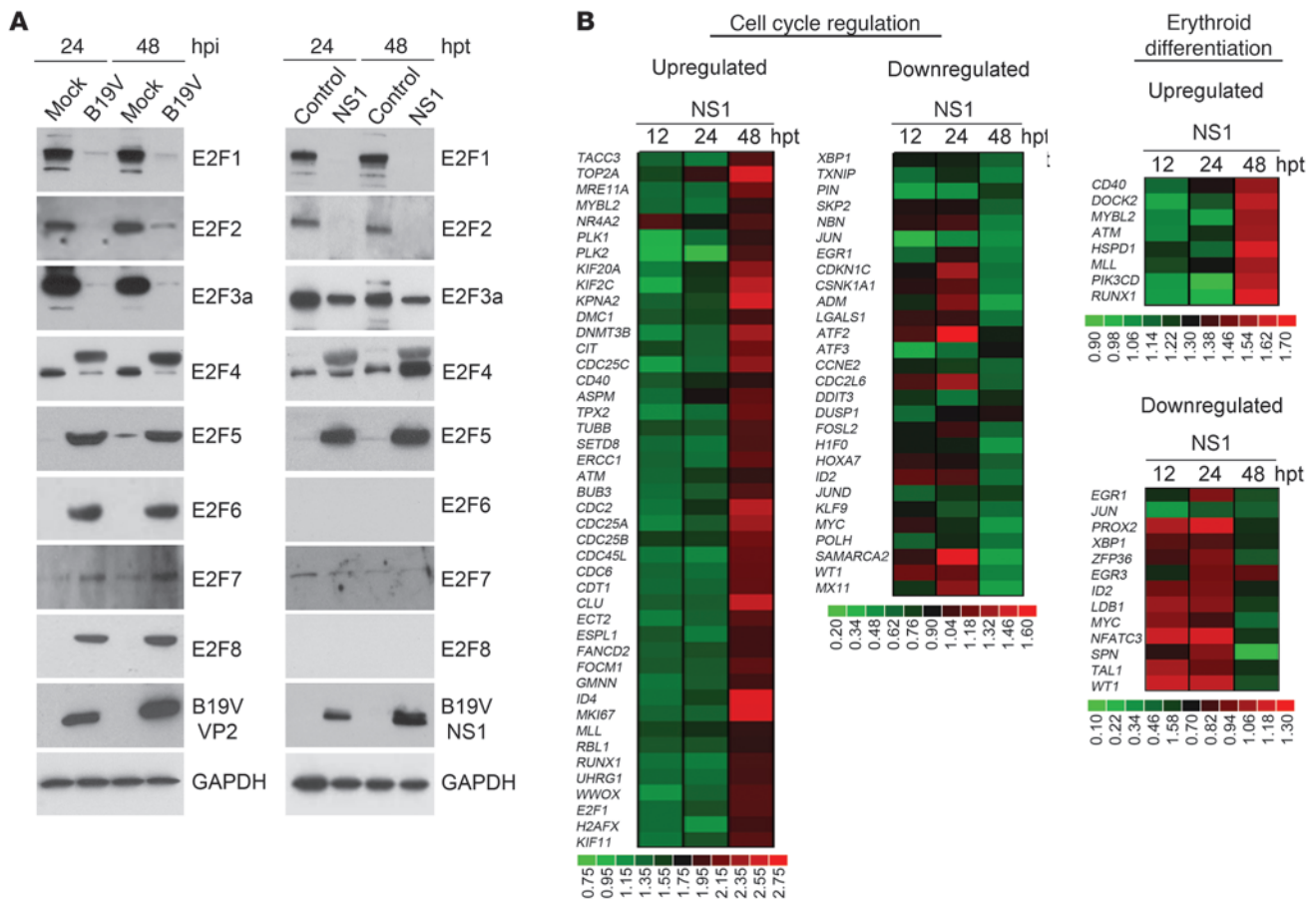


Figure 2 B19V NS1 protein regulates the E2F family of transcription factors. (A) Immunoblot analysis of E2F transcription factors. CD36+ EPCs were B19V- or mock-infected or transduced with NS1 or control lentivirus. Whole cell lysates were prepared at the indicated time points, resolved on 4%–12% SDS-PAGE, and subjected to immunoblot analysis with antibodies specific for individual E2Fs, B19V VP2, Flag (NS1), or GAPDH. (B) Transcription profiles of E2F target genes affected by NS1. CD36+ EPCs were transduced with NS1 or control lentivirus, followed by total RNA isolation at the indicated time points and then microarray analysis using Affymetrix HG-U133 Plus 2 arrays as described in Methods. Among 1,045 genes with greater than 1.5-fold changes, 93 were identified as E2F targets. Among them, 72 genes were involved in cell cycle regulation (44 upregulated and 28 downregulated) and 21 genes (8 upregulated and 13 downregulated) in cell differentiation. The heat map represents normalized intensity (NS1 divided by control) for each time point. Gene symbols are listed to the left of each panel.

time point were further analyzed with Ingenuity software (Ingenuity Systems). Of the 1,045 differentially expressed genes, 177 were involved in cell cycle regulation (Supplemental Table 8), of which 72 genes (28 downregulated and 44 upregulated) were previously characterized as the targets of E2Fs (Figure 2B). Expression levels of 12 downregulated E2F target genes were validated by real-time RT-PCR (Table 1). Among these downregulated E2F targets, *MYC* (37) and *WT1* (38) have been previously shown to be involved in G₂/M transition. In NS1-transduced CD36+ EPCs, both *MYC* and *WT1* expression continuously decreased in a time-dependent fashion by similar levels (~3-fold) at 24 hpt and by approximately 4- and 9-fold at 48 hpt. *HIF0*, a member of the histone H1 family, exhibited the most dramatic decrease among these E2F target genes, with approximately 2-, 7-, and 29-fold decreases at 12, 24, or 48 hpt, respectively. Further, 5 transcription factors (*SMARCA2/BRG1*, ref. 39; *HOXA7*, ref. 40; *KLF9*, ref. 41; *JUND*, ref. 42; and *FOSL2*, ref. 43) that are involved in regulation of cell cycle progression also displayed markedly decreased expression in NS1-transduced CD36+ EPCs.

In addition to cell cycle regulation, ontology analysis revealed that 51 differentially expressed genes were involved in the regulation of cell differentiation (Supplemental Table 9), 21 of which (13 downregulated and 8 upregulated) were previously characterized as E2F targets (Figure 2B). Among 13 downregulated E2F4/E2F5 targets, we selectively validated expression levels of *TAL1*, *SPN*, *JUN*, *MYC*, *WT1*, and *EGR3* by real-time RT-PCR, due to their important roles in erythroid progenitor differentiation (Table 1). Expression of *TAL1*, a transcription factor-regulating gene involved in erythroid differentiation (44, 45), exhibited a time-dependent decrease in NS1-transduced cells, with approximately 1.5-, 1.7-, and 3.1-fold decreases at 12, 24, and 48 hpt, respectively. *SPN* (CD43) is considered to be a hematopoietic marker for differentiating erythroid progenitors (46). In parallel with a decreased expression of *TAL1*, *SPN* was considerably downregulated in NS1-transduced cells, suggesting an NS1 inhibitory effect on CD36+ EPC differentiation. Reduced expression of *EGR3*, a zinc-finger transcription factor



Table 1
Expression changes of E2F4/E2F5 target genes relating to cell cycle control and erythroid differentiation

Gene symbol	Fold change ^A				Description	Gene ID
	6 h	12 h	24 h	48 h		
<i>H1FO</i>	-1.4	-2.2	-6.7	-28.9	H1 histone family, member 0	3005
<i>HOXA7</i>	-1.2	-9.9	-18.3	-19.6	Homeobox A7	3204
<i>EGR3</i>	-2.1	-8.4	-7.6	-17.6	Early growth response 3	1960
<i>WT1</i>	-1.4	-1.0	-2.6	-8.6	Wilms tumor 1	7490
<i>DDIT3</i>	-1.2	-1.0	-1.7	-5.6	DNA-damage-inducible transcript 3	1649
<i>SPN</i>	-1.1	-1.3	-1.1	-5.6	Sialophorin	6693
<i>JUND</i>	-1.6	-3.8	-8.0	-4.9	Jun D proto-oncogene	3727
<i>SMARCA2</i>	-1.4	-2.7	-2.9	-4.4	Regulator of chromatin, subfamily a, member 2	6595
<i>ATF3</i>	1.4	1.6	1.9	-4.0	Activating transcription factor	467
<i>DUSP1</i>	-2.0	-2.7	-5.1	-3.9	Dual specificity phosphatase 1	1843
<i>MYC</i>	-1.5	-2.1	-3.0	-3.6	Myelocytomatosis viral oncogene homolog	4609
<i>CDC2L6</i>	-1.0	-1.0	-9.3	-3.3	Cell division cycle 2-like 6	23097
<i>KLF9</i>	-1.6	-1.7	-4.1	-3.1	Kruppel-like factor 9	687
<i>TAL1</i>	-1.1	-1.5	-1.7	-3.1	T cell acute lymphocytic leukemia 1	6886
<i>FOSL2</i>	-1.5	-2.3	-2.4	-2.8	FOS-like antigen 2	2355
<i>ACTB</i>	-1.0	1.1	1.0	1.1	Actin, beta	60
<i>B2M</i>	1.1	1.0	-1.1	1.9	Beta-2-microglobulin	567
<i>HPRT1</i>	-1.5	-1.1	-1.1	1.0	Hypoxanthine phosphoribosyltransferase 1	3251
<i>RPL13A</i>	1.2	-1.1	1.0	1.1	Ribosomal protein L13a	23521

^AFold change represent ratios of gene expression levels of NS1-transduced cells at different time points (6, 12, 24, and 48 hpt), compared with controls.

involved in cellular growth and differentiation (47), was also observed at any time points tested in NS1-transduced cells.

Association of NS1 with E2F4 or E2F5 enhances their nuclear import. To elucidate a mechanism by which NS1 induced E2F4 and E2F5 accumulation, CD36⁺ EPCs were transduced with either NS1 or control lentivirus and subjected to coimmunoprecipitation assays using anti-E2F4 or anti-E2F5 antibody and then anti-Flag (NS1) antibody. As shown in Figure 3A, coprecipitation of NS1 with endogenous E2F4 or E2F5 was detected, indicating an association of NS1 with E2F4 or E2F5. To ascertain a potential association of a pocket protein with an NS1-E2F4 complex, we performed coimmunoprecipitation assays with antibody for E2F4 or Flag (NS1), followed by immunoblotting with antibody for each pocket protein, E2F4, or Flag (NS1). The 3 pocket proteins and Flag (NS1) were identified within E2F4 immunoprecipitate (Figure 3B). As expected, E2F4 was also identified in Flag (NS1) immunoprecipitate, but pRb, p130, and p107 were not detected (Figure 3B). Thus, the E2F4-NS1 complex coexisted with E2F4-pRb, E2F4-p130, and E2F4-p107 complexes in NS1-transduced CD36⁺ EPCs, but a tri-complex (for example, E2F4-NS1-pRb) was undetectable.

When examined by confocal microscopy, E2F4 and E2F5 were mainly cytoplasmic in control cells (Figure 3C). In NS1-transduced cells, expression of E2F4 and E2F5 increased in both cytoplasm and nucleus at 24 hpt, while the NS1 protein was predominantly localized in nucleus, with apparent colocalization with E2F4 or E2F5, indicating direct involvement of NS1 in alteration of E2F4 and E2F5 subcellular localizations. To further define the relationship between E2F4/E2F5 and NS1, we collected a series of z-stacks throughout cells and analyzed the 3D data. Images were deconvolved, and 3D renderings are presented in Figure 3D, in which a white mask in a merged image reveals colocalized pixels. In addition to performing visual inspection, we quantified the colocalization. This analysis indicated a greater colocal-

ization of E2F5 and NS1, compared with E2F4 and NS1, with colocalization coefficients of 0.6 and 0.3, respectively (1, perfect correlation; 0, no correlation) (Figure 3D, 2D fluorograms).

B19V 11-kDa and 7.5-kDa proteins do not induce cell cycle arrest in CD36⁺ EPCs. In addition to NS1, the B19V genome encodes two other small nonstructural proteins: 11-kDa and 7.5-kDa proteins. We examined a possible contribution of the 11-kDa or 7.5-kDa protein to B19V-induced cell cycle arrest by transducing CD36⁺ EPCs with 11-kDa, 7.5-kDa, or control lentivirus. In comparison with the control, cell cycle analysis revealed that neither 11 kDa nor 7.5 kDa had an obvious impact on cell cycle progression of the transduced cells at any time points tested (Figure 4A).

To elucidate whether B19V 11-kDa protein was able to enhance expression of E2F4 and E2F5, we subjected CD36⁺ EPCs transduced with 11-kDa or control lentivirus to immunoblot analysis with anti-E2F4 or anti-E2F5 antibody. Expression levels of E2F4 and E2F5 in 11-kDa-transduced cells were similar to those in control cells (Figure 4B), indicating that the 11-kDa protein was unable to increase E2F4 and E2F5 expression. To assess a possible association between the 11-kDa protein and E2F4 or E2F5, we carried out a coimmunoprecipitation assay using anti-E2F4 or anti-E2F5 antibody and then anti-Flag (11 kDa) antibody. As shown in Figure 4B, coprecipitation of the 11-kDa protein with E2F4 or E2F5 was not detected. Moreover, IF analysis was performed to examine whether the nuclear translocation of E2F4 and E2F5 also occurred in 11-kDa-transduced CD36⁺ EPCs. Confocal analysis showed that the 11-kDa protein was exclusively localized in cytoplasm, and no nuclear accumulation of E2F4 or E2F5 was observed (Figure 4C). Taken together, the data suggest that NS1 is a major player in cell cycle arrest among the three B19V nonstructural proteins.

NS1-dependent nuclear translocation of E2F4 or E2F5 causes stable G₂ arrest, which augments B19V replication. To investigate whether nuclear localization of E2F4 or E2F5 was mediated by the nuclear import abil-

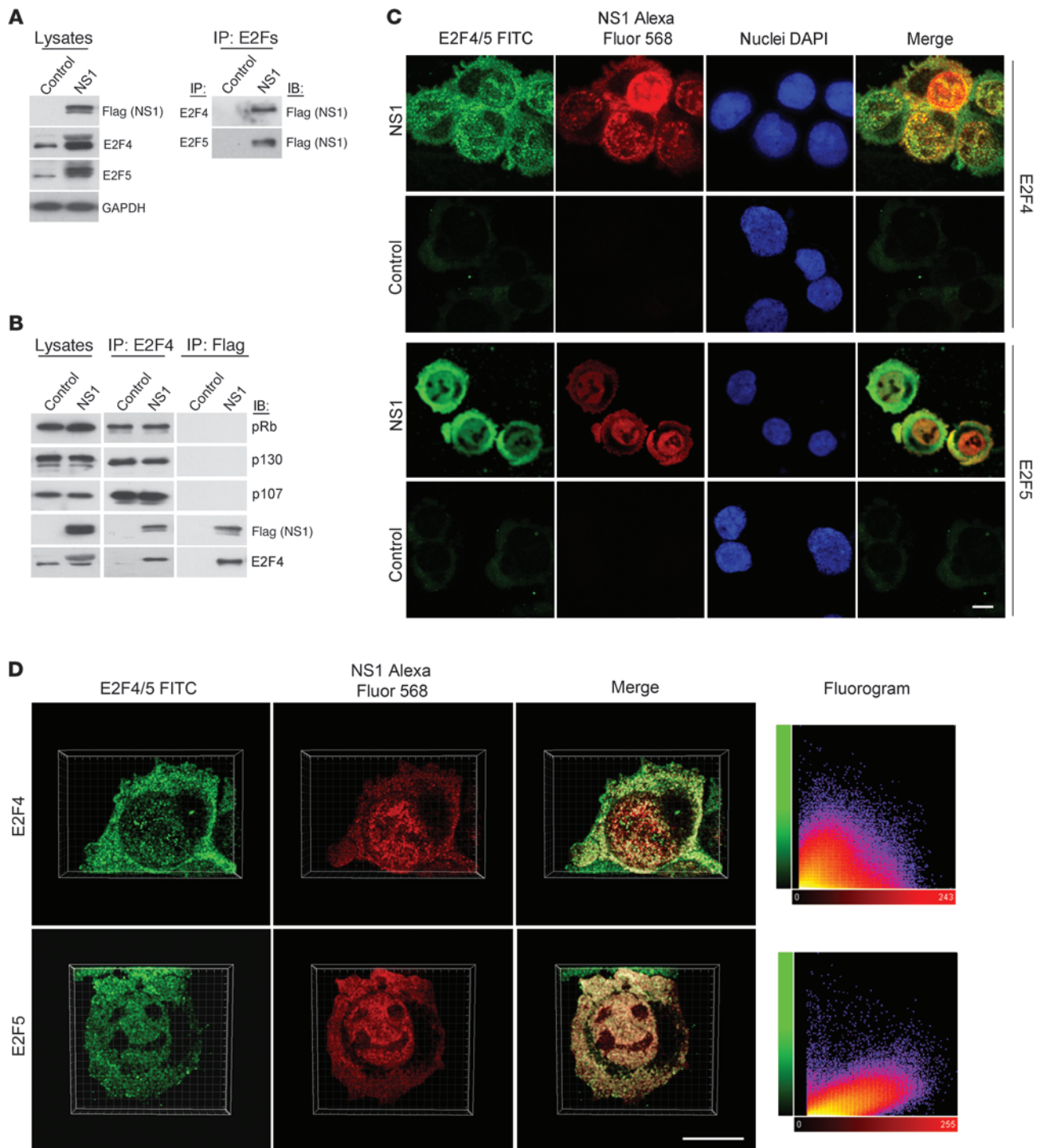


Figure 3

B19V NS1 protein enhances the nuclear import of E2F4 and E2F5 by formation of a heterocomplex. NS1-transduced CD36⁺ EPCs were harvested at 24 hpt for subsequent experiments. **(A)** Whole cell lysates were subjected to immunoprecipitation by incubation with anti-E2F4 or anti-E2F5 antibody and then immunoblotting with anti-Flag (NS1) antibody. **(B)** Whole cell lysates were subjected to immunoprecipitation with anti-E2F4 or anti-Flag (NS1) antibody and subsequently analyzed by immunoblotting with the indicated antibodies. Whole cell lysates (5% input) without immunoprecipitation were also analyzed by immunoblotting as controls. **(C)** Cells were immunostained with antibody against E2F4, E2F5, or Flag (NS1), followed by secondary antibody conjugated with FITC (green) for individual E2Fs or with Alexa Fluor 568 (red) for Flag (NS1). After counterstaining of nuclei with DAPI (blue), cells were examined by confocal microscopy. **(D)** To address the relationship between E2F4/5 and NS1, z-series were collected throughout cells, and the 3D data were analyzed. Images were deconvolved, and the 3D renderings are shown. 2D fluorograms represent quantification of the colocalization of E2F4 or E2F5 with NS1: colocalization coefficients of 0.6 (E2F5 and NS1) and 0.3 (E2F4 and NS1) (1, perfect correlation; 0, no correlation; -1, perfect inverse correlation). Scale bars: 10 μ m.

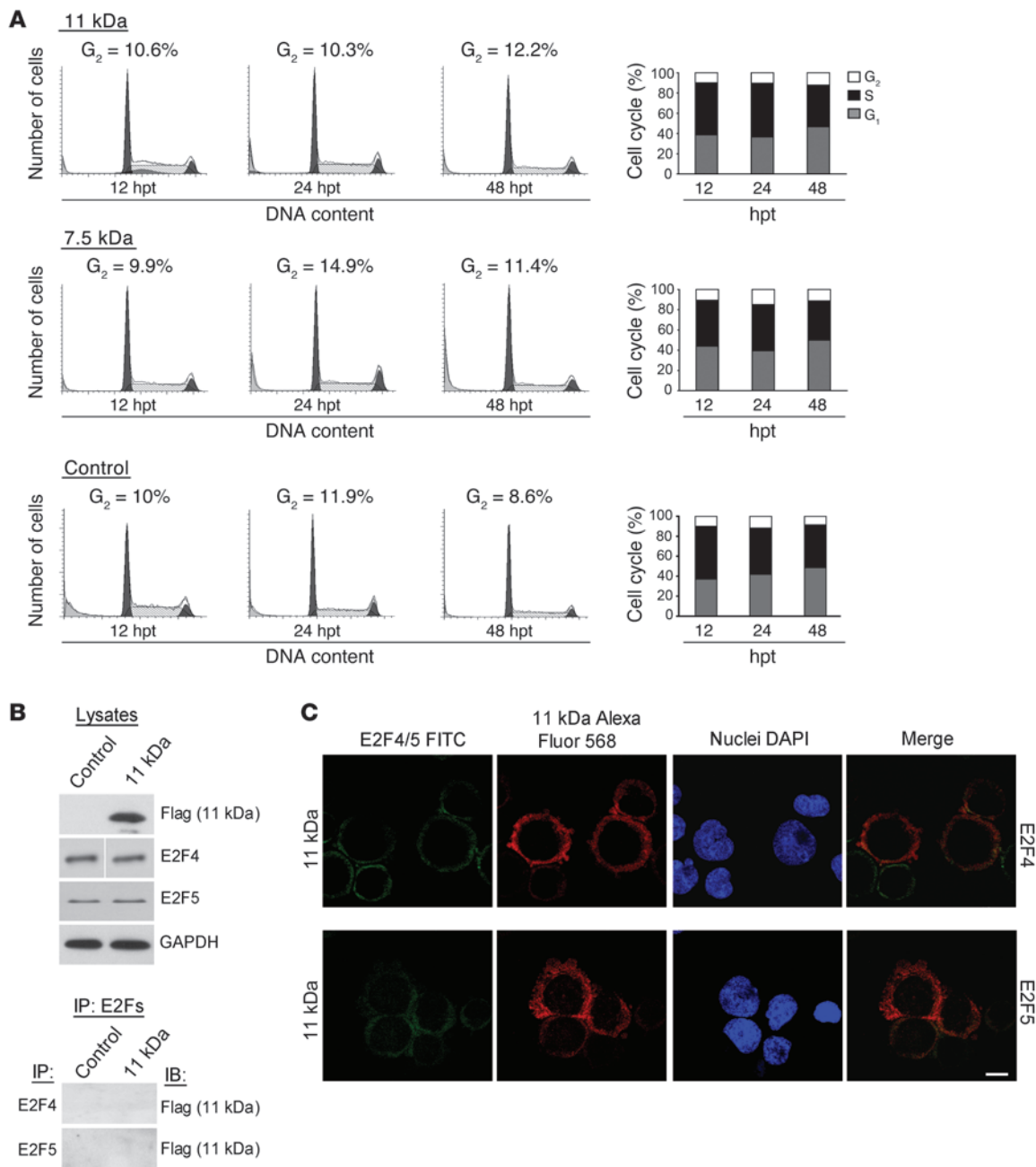


Figure 4

B19V 11-kDa and 7.5-kDa proteins do not induce cell cycle arrest in CD36⁺ EPCs. **(A)** Cells transduced with 11-kDa or 7.5-kDa lentivirus were subjected to cell cycle analysis by measuring DNA content at the indicated time points. On the right, percentages of cells in different phases of cell cycle are presented with respect to time points. Similar results were obtained in duplicate experiments. **(B)** Whole cell lysate prepared from cells transduced with 11-kDa or control lentivirus was analyzed by immunoprecipitation with anti-E2F4 or anti-E2F5 antibody, followed by immunoblotting with anti-Flag (11 kDa) antibody. Individual whole cell lysates (5% input) without immunoprecipitation were also analyzed by immunoblotting as controls. The images to the left and right of the vertical white line are derived from nonadjacent lanes on the same blot. **(C)** Cells were immunostained with antibody against E2F4, E2F5, or Flag (11 kDa), followed by secondary antibody conjugated with FITC (green) for individual E2Fs or with Alexa Fluor 568 (red) for Flag (11 kDa). After counterstaining of nuclei with DAPI (blue), cells were examined by confocal microscopy. Scale bar: 10 μm.

ity of B19V NS1, we sought to create an NS1 mutant that was unable to translocate into nucleus. We first employed a Web-based program (see Methods) to search for an NLS in the NS1 protein and found a cluster of basic amino acid residues (KKRP) between amino acids 177 and 180, which was homologous to the consensus sequence of eukary-

otic NLS. To confirm a function of this putative NLS, we introduced a substitution mutation of K177C into NS1 by site-directed mutagenesis (Figure 5A). The NS1 mutant carrying the substitution mutation (K177C) was designated as NS1mt. In contrast to the predominant nuclear localization of NS1, the NS1mt protein was exclusively local-



ized in the cytoplasm in transduced cells (Figure 5A), confirming that NLS in B19V NS1 was operational. In addition, NS1mt was unable to induce nuclear translocation of E2F4 and E2F5, although it was still functional for the upregulation of their expression (Figure 5B). To assess the nuclear-cytoplasmic distribution of E2F4 and E2F5, we further analyzed confocal images by drawing an intensity line profile of cells in transverse section; fluorescence intensities of the 3 channels were displayed as histograms, in which a DAPI line graph (blue) was used to localize the nucleus. In NS1-transduced CD36⁺ EPCs, E2F4 and E2F5 line graphs (green) reproducibly followed the NS1 line graph (red), over cytoplasm and enriched over the nucleus, but in NS1mt-transduced cells, both NS1 and E2F4 or E2F5 were markedly redistributed toward cytoplasm (Figure 5C). Nonetheless, coimmunoprecipitation analysis showed that NS1mt still maintained ability to associate with E2F4 or E2F5 (Figure 5D).

Next, we measured proliferation of CD36⁺ EPCs after NS1 or NS1mt lentivirus transduction. In comparison to the control cells, both NS1 and NS1mt transductions largely inhibited CD36⁺ EPC proliferation. However, the inhibitory effect was much stronger in the case of NS1 than NS1mt (Figure 6A and Supplemental Table 4). Moreover, although the ratio of dead cells gradually increased (25% and 21% by day 2 in NS1- and NS1mt-transduced cells, respectively), there was no obvious difference in the ratio of dead cells between in NS1- and NS1mt-transduced cells. In contrast to the time-dependent G₂ arrest induced by NS1, cell cycle progression appeared to be normal in NS1mt-transduced cells, with 9.2%, 19%, and 15% of cells in G₂ at 12, 24, and 48 hpt, respectively (Figure 6B and Supplemental Table 5). These results strongly suggest that NS1-dependent nuclear translocation of E2F4 and E2F5 is essential for perturbation of cell cycle progression.

NS1 is known to induce apoptosis during B19V infection. In attempt to test whether NS1mt without nuclear translocation was still able to induce apoptosis in CD36⁺ EPCs, we performed apoptosis analysis of NS1- or NS1mt-transduced or B19V-infected CD36⁺ EPCs using annexin V/propidium iodide (PI) double staining. Flow cytometric analysis showed a time-dependent increase in apoptotic cells: 14%, 25%, and 36% apoptotic cells at 12, 24, and 48 hpi, respectively in NS1-transduced cells; and 17%, 22%, and 37% at 12, 24, and 48 hpi, respectively, in NS1mt-transduced cells (Figure 7A). In contrast, the ratio was similar in control cells in the time course examined. Our results indicate that NS1 and NS1mt induce similar ratios of apoptosis or cell death at any time points tested, but their inhibitory effects on cell proliferation are different. In comparison with NS1 or NS1mt transduction, B19V infection induced a higher ratio of apoptotic cells, by 28% and 49% at 24 and 48 hpi, respectively (Figure 7B). Interestingly, B19V-infected cells displayed a much higher percentage of cells in early apoptosis (annexin V-positive) than late apoptosis (annexin V- and PI-positive) at all time points examined, in contrast to NS1- or NS1mt-mediated apoptosis, suggesting participation of other B19V elements that may compensate for the effect of NS1-related cytotoxicity.

To investigate a functional role of E2F4 or E2F5 nuclear translocation, lentivirus carrying E2F4 siRNA or E2F5 siRNA was generated and transduced into CD36⁺ EPCs, resulting in a substantial decrease in the level of E2F4 or E2F5 (Supplemental Figure 3). We next examined the cell cycle profile for NS1-transduced CD36⁺ EPCs by pretreatment (24 hours) with E2F4 siRNA or E2F5 siRNA lentivirus. When compared with nonsilencing siRNA and GAPDH siRNA controls, the proportion of G₂-arrested cells was significantly reduced in E2F4 siRNA-treated cells (31% at 24 hpt and 46% at 48 hpt) and

E2F5 siRNA-treated cells (14% at 24 hpt and 27% at 48 hpt), concomitant with enhanced proportions of G₁- and S-phase cells (Figure 8A and Supplemental Table 6). No substantial change in cell cycle progression was observed in control cells that were treated with each siRNA alone — E2F4, E2F5, nonsilencing, or GAPDH — but without subsequent NS1 transduction. These results demonstrate that knockdown of E2F4 or E2F5 abrogates NS1-induced G₂ arrest.

To further investigate whether G₂ arrest induced by B19V infection was advantageous for viral replication, E2F4 siRNA- or E2F5 siRNA-treated cells were infected with B19V and subjected to real-time PCR and real-time RT-PCR to assess viral DNA replication and RNA transcription, respectively. As shown in Figure 8, B and C, both viral DNA and RNA production were lower in E2F4 siRNA- and E2F5 siRNA-treated cells than in nonsilencing siRNA-treated cells. To evaluate the impact of knockdown of E2F4 or E2F5 on infectious progeny virion production, CD36⁺ EPCs were infected with lentivirus carrying siRNA against E2F4 or E2F5 and incubated for 24 hours, followed by B19V infection. At 72 hpi, cells were subjected to 3 cycles of freeze-thaw and then low-speed centrifugation. Clarified supernatants were serially diluted and used for further infection of CD36⁺ EPCs. At 72 hpi, infectious titers were determined by end-point 10-fold serial dilution analysis, in which B19V capsid and B19V NS1 transcripts were measured by real-time RT-PCR with appropriate primers and probes. E2F4 siRNA- or E2F5 siRNA-treated CD36⁺ EPCs produced 10-fold-lower numbers of infectious B19V particles than nonsilencing lentivirus-transduced cells, revealing that suppression of E2F4 and E2F5 had a negative impact on B19V virion production. Taken together, these results indicate that NS1-induced G₂ arrest is beneficial for B19V replication in CD36⁺ EPCs.

NS1-induced G₂ arrest is independent of p53 signal transduction. Since p53 plays a crucial role in cell cycle arrest induced by DNA damage response, immunoblot analysis was conducted to address expression and activation of p53 as well as p21^{WAF1/CIP1} (a key factor immediately downstream of p53) in B19V-infected or NS1-transduced CD36⁺ EPCs. B19V infection not only enhanced p53 production but also induced its phosphorylated form (at Ser15 or Ser20, an active form of p53) at both 24 and 48 hpi, compared with controls (Figure 9). In parallel with the activation of p53, the level of p21^{WAF1/CIP1} was first elevated at 24 hpi in infected cells and peaked at 48 hpi. For NS1-transduced cells, p53 expression and its phosphorylation levels (at both Ser15 and Ser20) remained unchanged, compared with control cells, whereas the p21 expression slightly increased at both 24 and 48 hpt, to a much lesser extent than in B19V-infected cells (Figure 9). Thus, NS1-induced cell cycle arrest does not appear to be dependent on p53 activation.

Discussion

Accumulating evidence has revealed that the G₁/S boundary is not the only transition targeted by viruses and that many viruses preferentially induce cell cycle arrest at G₂/M (48). The G₂ checkpoint acts to prevent cells from entering mitosis in response to DNA damage, thereby providing an opportunity for repair and halting proliferation of damaged cells. The p53 and pRb families of transcriptional repressors play critical roles in G₂ arrest by downregulating a large number of genes involved in the G₂/M transition. Although the benefits of G₂ arrest to the viral life cycle remain unclear, recent studies have suggested that viruses have aggressively evolved mechanisms to “hijack” cellular DNA repair proteins to aid in their own replication or to use G₂-related transcription factors to enhance viral protein synthesis.

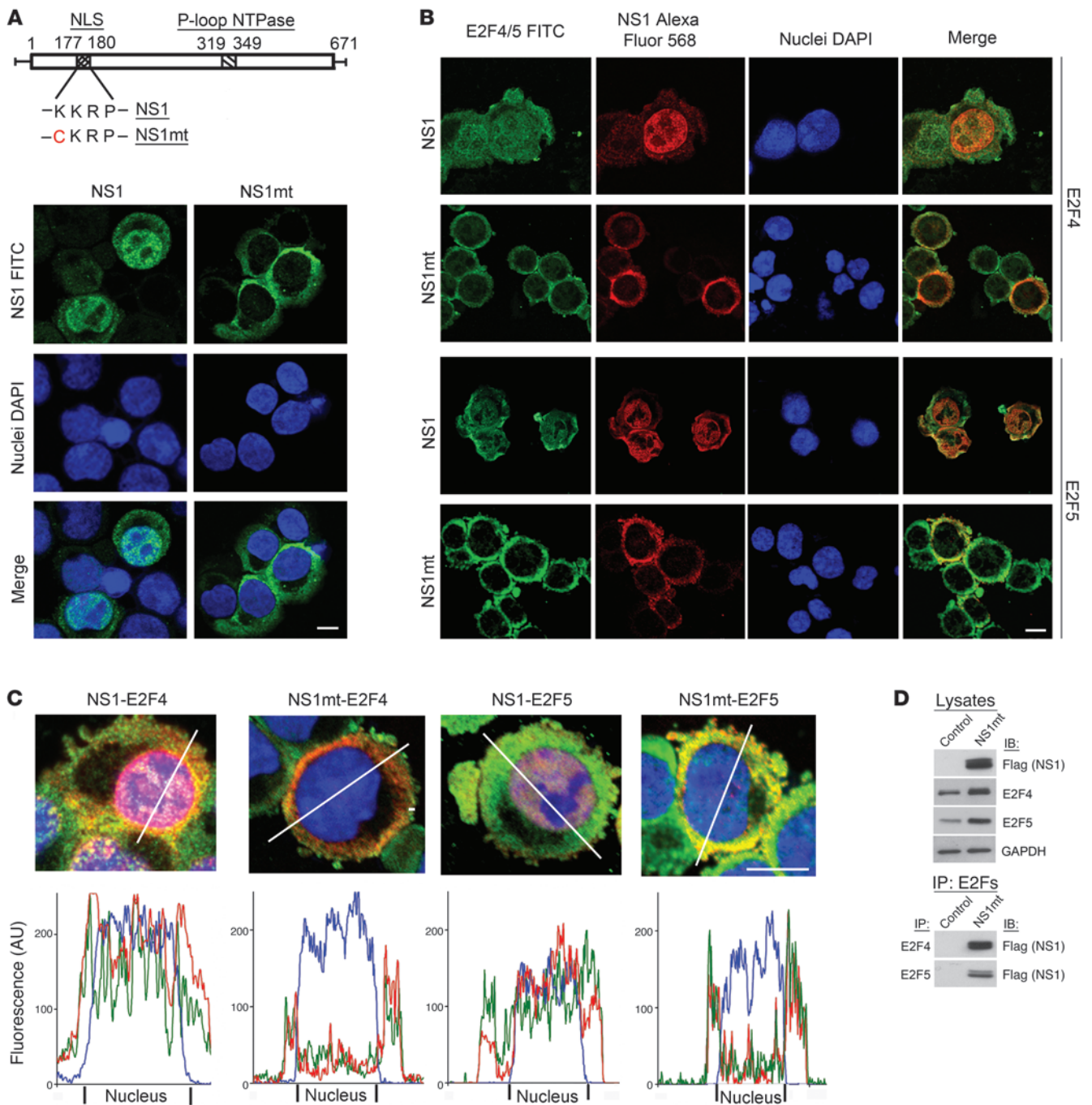


Figure 5

Identification of the NLS of NS1 and its impact on the nuclear translocation of E2F4 and E2F5. CD36⁺ EPCs were transduced with lentivirus carrying NS1, NS1mt (K177C), or vector alone and harvested at 24 hpt for subsequent analyses. **(A)** Top: Schematic diagram of a putative NLS motif in NS1 and the position of the substitution mutation (K177C). Bottom: Cells were immunostained with anti-Flag (NS1) antibody and then with FITC-conjugated secondary antibody (green). After counterstaining of nuclei with DAPI (blue), cells were observed by confocal microscopy. **(B)** Cells were immunostained with anti-E2F4 or anti-E2F5 antibody and then with FITC-secondary antibody (green) or immunostained with anti-Flag (NS1) antibody and then with Alexa Fluor 568-secondary antibody (red). **(C)** Confocal images were analyzed by drawing an intensity line profile of cells in transverse section; fluorescence intensities of the 3 channels were plotted as histograms. A DAPI histogram is shown in blue for localizing the nucleus. Histograms of NS1 and E2F4 or E2F5 are shown in red (Alexa Fluor 568) and green (FITC), respectively. **(D)** Whole cell lysates prepared from NS1mt- or control-transduced cells were subjected to immunoprecipitation with anti-E2F4 or anti-E2F5 antibody, followed by immunoblotting with anti-Flag (NS1) antibody. Whole cell lysates (5% input) without immunoprecipitation were also analyzed by immunoblotting as controls. Scale bars: 10 μm.

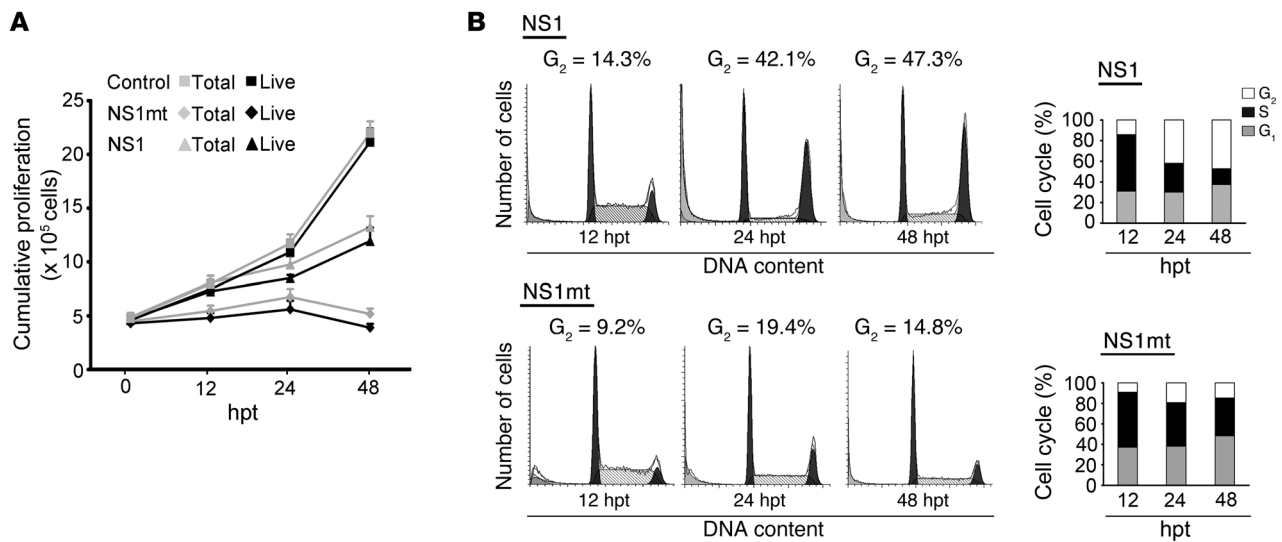


Figure 6 Cell proliferation analysis of NS1- or NS1mt-transduced CD36⁺ EPCs. **(A)** Cumulative proliferation of NS1- or NS1mt-transduced cells was measured by counting live or dead cells using the trypan blue exclusion method, and results are presented as total and live cell numbers. Data are expressed as mean ± SD of 3 independent experiments. **(B)** Cell cycle profiles were measured by staining of DNA content at the indicated time points by flow cytometry. On the right, percentages of cells in different cell cycle phases are presented with respect to time points. Similar results were obtained in duplicate experiments.

Few studies on the viral G₂/M arrest have been conducted during natural viral infection (49, 50). Since most experiments have been performed in transformed cell lines for convenience, the actual biological effects of viral proteins may be masked as these cells often exhibit abnormal cell cycle signaling. This methodological difficulty may be particularly problematic for B19V. The majority of studies on B19V-induced cellular changes have used several semi-permissive cell lines (18, 19) that are not only derived from tumor cells but also exhibit a low rate of viral infectivity (less than 10%), with limited viral production. Due to its restricted tropism for EPCs, there are no fully permissive cell lines for B19V propagation. Here, we employed the primary CD36⁺ EPC-based culture system, which generates fully permissive cells for B19V propagation (36). Upon B19V infection or NS1 transduction, CD36⁺ EPCs displayed G₂ arrest in a time-dependent manner. However, in previous studies, B19V infection has led to G₂ arrest in UT7/Epo-S1 cells, a semi-permissive megakaryocytic leukemia cell line (18), whereas NS1 expression primarily induced G₁ arrest (19) in these cells. In contrast, our current data showed that B19V-induced G₂ arrest in the primary CD36⁺ EPCs was mediated by NS1-dependent E2F4/E2F5 nuclear translocation as well as repression of E2F4/E2F5 target genes. Although the detailed molecular mechanisms remain unclear, this discrepancy may be due to the different cell types, megakaryocytic leukemia cells (UT7/Epo-S1) versus primary EPCs. While exactly mimicking the expression of viral genes in native viral infection is problematic in any reductionist experiment, the advantages of studying the function of a viral protein in relative isolation include the avoidance of these practical difficulties and the clarity that results from adequately controlled experiments. In the present study, we employed the lentivirus-based transduction system to investigate the role of B19V NS1 in host cell cycle perturbation and found that the NS1 protein induced stable G₂ arrest by enhancing nuclear import of E2F4 and E2F5. Although there was a slightly increased G₂ population in the cells transduced with control len-

tivirus in comparison to mock-infected cells, these changes were much less extensive and not time dependent, as were those detected in NS1-transduced cells. Moreover, in contrast to B19V infection or NS1 transduction, control lentivirus (empty vector) did not induce changes in expression of E2Fs, nor did it impact p53 activation. Therefore, we believe that the minor changes induced by control lentivirus are unlikely to influence interpretation of results for B19V NS1-induced cell cycle arrest. To avoid the artifacts caused by overexpression of NS1, we evaluated NS1 transcription by real-time RT-PCR to ensure that the level of NS1 expression in transduced cells was similar to that resulting from native B19V infection. Meanwhile we also performed a similar analysis on the other two B19V nonstructural proteins (11 kDa and 7.5 kDa) and ruled out their potential roles in the cell cycle perturbation caused by B19V. We further showed that siRNA-mediated E2F4/E2F5 knockdown partially blocked NS1-induced G₂ arrest and decreased viral production in CD36⁺ EPCs. Therefore, it is evident that NS1 is a major player in B19V-induced G₂ arrest, which provides a favorable environment for B19V replication.

Our current work provides evidence that B19V exploits the E2F family of transcription factors by downregulating activating E2Fs (E2F1, E2F2, and E2F3a) and upregulating repressive E2Fs (E2F4, E2F5, E2F6, E2F7, and E2F8). Specifically, the interaction of NS1 with E2F4 or E2F5 led to their predominant accumulation in nucleus, resulting in the impaired cell cycle progression of the primary CD36⁺ EPCs. Despite the fact that they are exported from the nucleus under normal conditions, E2F4 and E2F5 appeared to be trapped in nucleus by NS1 binding. E2F4 and E2F5 compared with other E2Fs are primarily cytoplasmic by association with CRM1 (51), and they contain a nuclear export signal. Heterodimerization of E2F4 (and presumably E2F5) with a pocket protein (pRb, p107, or p130) is responsible for nuclear import and accumulation of E2F4 in the nucleus in the G₀/G₁ phase of the cell cycle (27). Of interest, our coimmunoprecipitation experiment

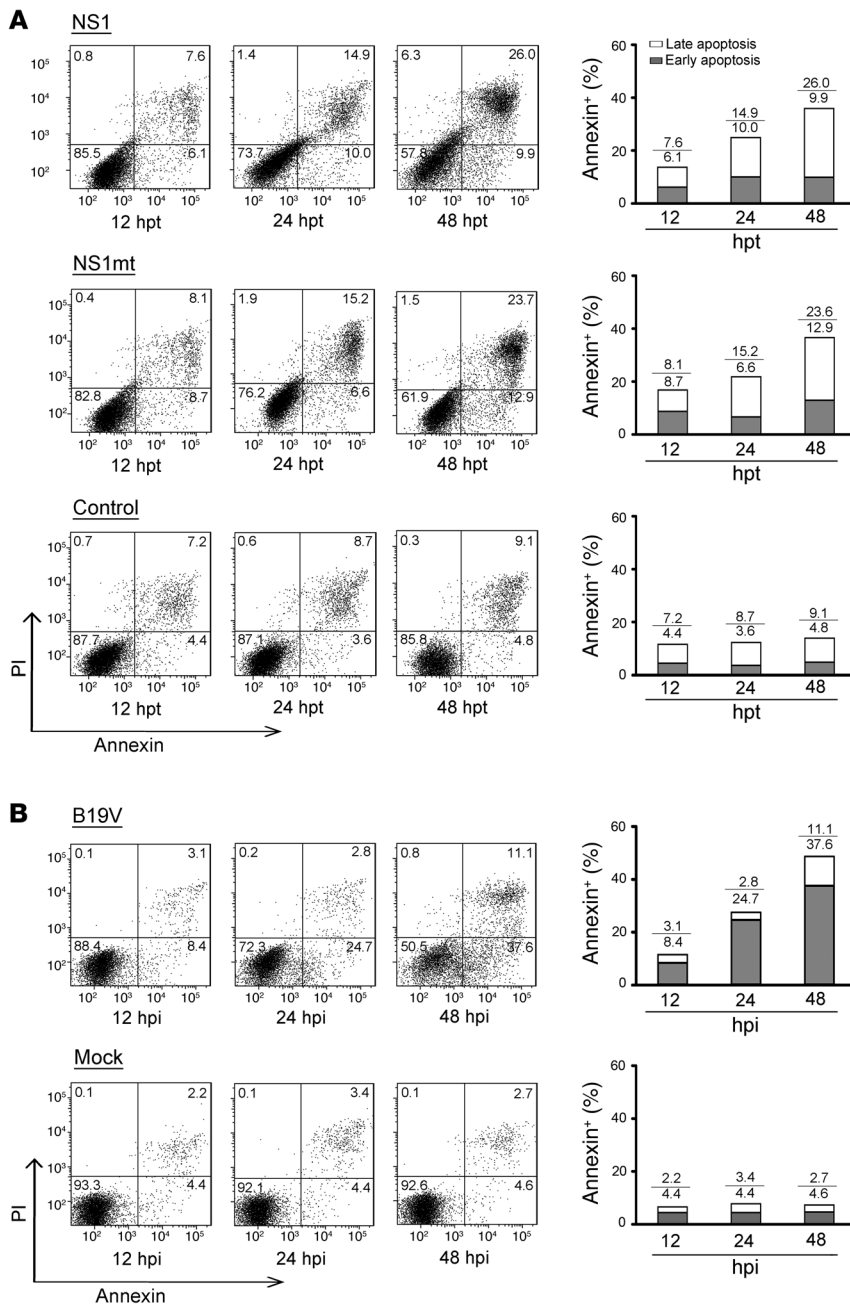


Figure 7

Apoptosis analysis of NS1-transduced, NS1mt-transduced, or B19V-infected CD36⁺ EPCs. (A) After transduction with NS1, NS1mt, or control lentivirus, cells were collected at the indicated time points and subjected to annexin V/PI double staining, followed by flow cytometry analysis. Numbers in each quadrant indicate the percentage of cells that were annexin V⁺/PI⁺, annexin V⁺/PI⁻, annexin V⁻/PI⁺, and annexin V⁻/PI⁻. Results are representative of 3 independent experiments. (B) Apoptosis of B19V- or mock-infected cells was assessed in manner similar to that described above. Percentages of cells in different apoptotic stages are shown on the right.

dependent on dissociation from pRb, p107, or p130 (53), although the precise mechanism is still unknown. NS1 binding may protect E2F4 and E2F5 from degradation, eventually contributing to the maintenance of transcriptional repression in the cells. Our real-time RT-PCR data support this hypothesis, as NS1 transduction induced downregulation of a group of E2F4/E2F5 target genes, many of which are transcription factors involved in the G₂/M transition and erythroid differentiation. Erythropoiesis is regulated by well-coordinated transcription factors that determine survival, proliferation, and differentiation of EPCs (54, 55). For its own replication and propagation, B19V appeared to abrogate the erythropoietic process by deregulation of a variety of transcription factors important for cell cycle control and differentiation.

Previous studies have described that the E2F4/p130 (and presumably E2F5/p130) colocalization in the nucleus leads to stable G₂ arrest in response to radiation-induced DNA damage (26) and that viral DNA replication stimulates DNA damage response (56). Since NS1 is critical to B19V DNA replication, NS1-mediated G₂ arrest in CD36⁺ EPCs might be a consequence of the DNA damage response. However, our results here and in previous studies indicate that NS1-

revealed that E2F4-pRb, E2F4-p107, and E2F4-p130 complexes were still present in NS1-transduced CD36⁺ EPCs, regardless of the nuclear accumulation of E2F4-NS1 and E2F5-NS1 complexes. It remains unclear whether these E2F4 and pocket protein complexes have some function in B19V propagation or crosstalk with NS1-E2F4 or NS1-E2F5 complexes. It is also unknown whether E2F4 and E2F5 display subtly different biological functions in B19V-infected CD36⁺ EPCs.

mRNA transcripts of both E2F4 and E2F5 remained unchanged or even slightly decreased at 24 hpt in NS1-transduced cells (Z. Wan and N. Zhi, unpublished observations), while the protein levels of E2F4 and E2F5 notably rose in cytoplasm and nucleus. E2F4 is known to be ubiquitinated and degraded by the proteasome in a manner

induced G₂ arrest is independent of the DNA damage response, at least in the context of NS1-transduced cellular machinery. First, we here detected time-dependent increases in E2F7, E2F8, p53, and p21 as well as the activation of p53 only in B19V-infected CD36⁺ EPCs, and not in NS1-transduced cells. This difference is likely due to the DNA damage response induced by viral DNA replication in B19V-infected cells because the repressive E2Fs (such as E2F7 and E2F8) as well as p53 and p21 have been previously shown to be induced in response to DNA damage (57, 58). Second, cell cycle analysis of B19V-infected CD36⁺ EPCs revealed accumulation (25% in infected versus 4.7% in mock-infected cells) of G₂-arrested cells in the early stage of the viral infection (12 hpi). In the B19V life cycle, synthesis of NS1 occurs much earlier than does either capsid

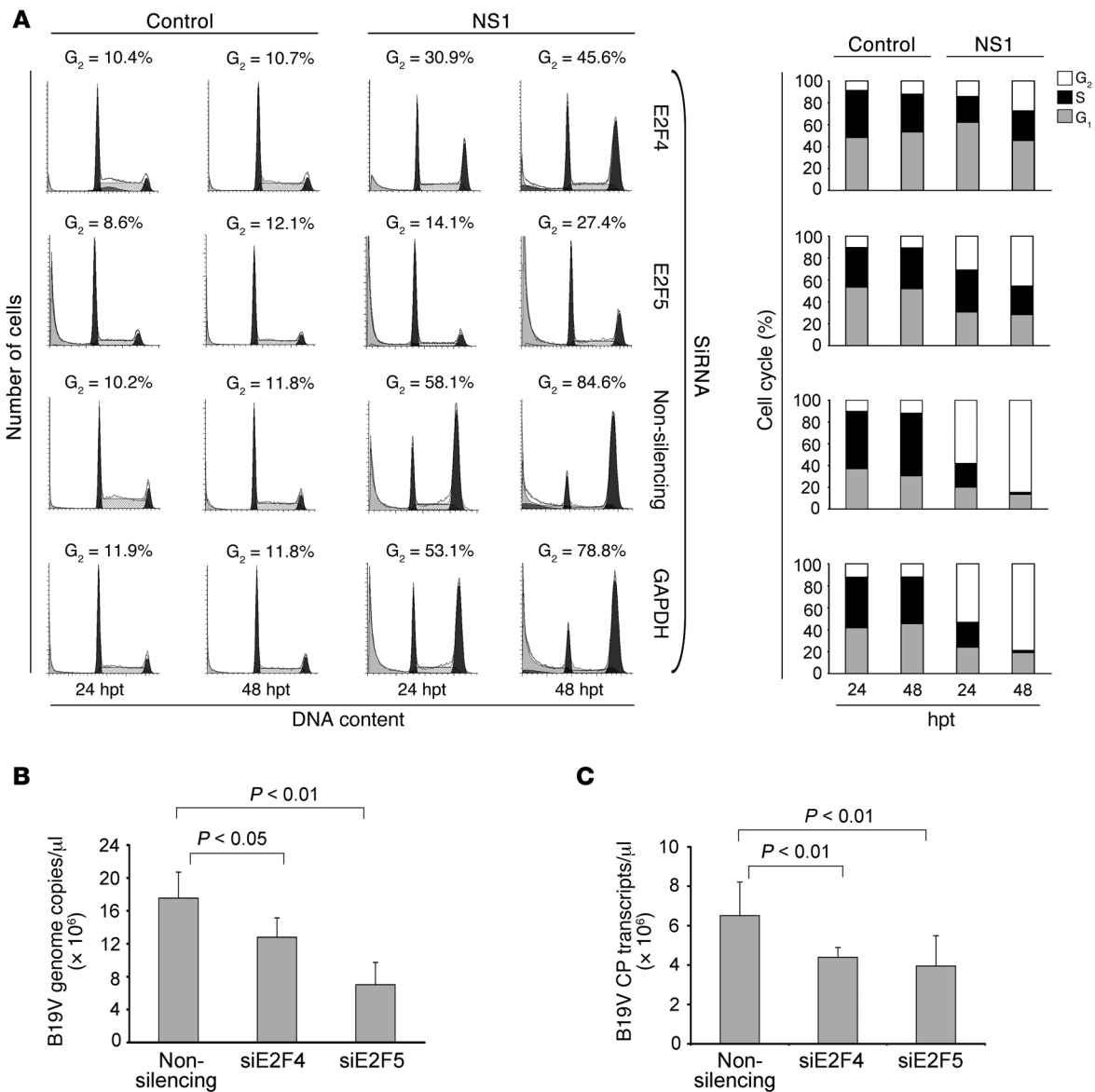


Figure 8 Downregulation of E2F4 or E2F5 by siRNA causes abrogation of NS1-induced G₂ arrest and inhibits B19V infection. **(A)** After treatment with individual siRNAs at an MOI of 20 for 24 hours, cells were transduced with NS1 or control lentivirus and then harvested at 24 hpt and 48 hpt. Cell cycle profiles were measured by staining for DNA content using flow cytometry, and percentages of cells in different cell cycle phases at indicated time points are presented on the right. Similar results were obtained in duplicate experiments. **(B and C)** After treatment with different siRNAs for 24 hours, cells were inoculated with approximately 5×10^{-1} infectious units/cell of B19V and collected at the indicated time points. Real-time PCR **(B)** or real-time RT-PCR **(C)** was performed to evaluate B19V DNA replication and RNA transcription, respectively, as described in Methods. Data are expressed as mean \pm SD of 3 independent experiments. CP, capsid protein.

production or DNA replication. RNA from the *NS1* gene appears at approximately 6 hpi, but replicative B19V genomes could not be detected until about 16 hpi (59). Active B19V replication and propagation, but not NS1 alone, appear mainly responsible for induction of the DNA damage response. NS1-dependent E2F4 and E2F5 nuclear translocations are likely early events and initiate G₂ arrest during B19V infection, allowing B19V to “hijack” host cell cycle regulation in order to create a favorable environment for its replication, although both induction of E2F7/E2F8 and activation of p53 may eventually contribute to G₂ arrest.

In summary, based on our results and other data, we propose a model mechanism for maximizing B19V replication and propagation in primary CD36⁺ EPCs (Figure 10). In early-stage B19V infection, interaction of NS1 with E2F4 or E2F5 induces exclusive redistribution of these repressive E2Fs to nucleus, leading to stable G₂ arrest and eventually impairing erythroid differentiation by downregulation of E2F target genes. Subsequently, activation of G₂-related transcription factors and/or DNA repair proteins enhances viral transcription and DNA replication. As B19V infection progresses, viral replication activates p53 signal transduction

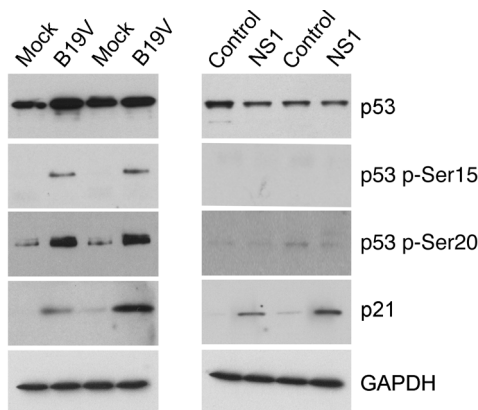


Figure 9
Immunoblot analyses of p53 and p21 in B19V-infected or NS1-transduced CD36⁺ EPCs. From B19V- or mock-infected cells, or NS1- or control lentivirus-transduced cells, whole cell lysates were prepared at 24 or 48 hpi or hpt and subjected to 4%–12% SDS-PAGE and then immunoblot analysis with respective antibodies.

and upregulates E2F7 and E2F8 in the context of the DNA damage response, blocking cell cycle progression. Thus, virus production would be maximized while simultaneously abrogating the cell's differentiation machinery.

Methods

Cell culture and B19V infection. Human CD36⁺ EPCs were generated as described in our previous study (36). 293T cells were maintained in DMEM containing 10% fetal bovine serum and antibiotics. Viremic plasma containing high-titer B19V (sample V1; 2 × 10¹² genome equivalents (ge)/ml, 1 infectious unit/2 × 10⁴ ge) was obtained from a normal blood donor, provided to our laboratory by Aris Lazo of VI Technologies (Watertown, Massachusetts, USA), and used to inoculate CD36⁺ EPCs with approximately 5 × 10⁻¹ infectious units/cell of B19V. The infection was carried out in a 96-well plate with 10 μl of cell culture (2 × 10⁴ cells) and 10 μl of the defined concentration of B19V. The infection was scaled up as necessary.

Lentiviral plasmid construction, lentivirus production, and lentivirus transduction. To construct a recombinant lentiviral plasmid encoding B19V NS1, the NS1 gene was first amplified by PCR from pB19V-PM20 carrying a full-length B19V genome (60) and then inserted into pCMV-3Tag-6 (Stratagene) in order to create a Flag-NS1 fusion protein (an N-terminal 3xFlag tag), resulting in pCMV-FlagNS1. The Flag-NS1 gene was PCR-amplified and cloned between *NaeI* and *NotI* sites in pCL20c MSCV-GFP (a gift from A. Nienhuis, St Jude Children's Research Hospital, Memphis, Tennessee, USA), generating pCL20c MSCV-FlagNS1 in which GFP was replaced with NS1. NS1 or control lentivirus was produced with pCL20c MSCV-FlagNS1 or pCL20c MSCV (a control)

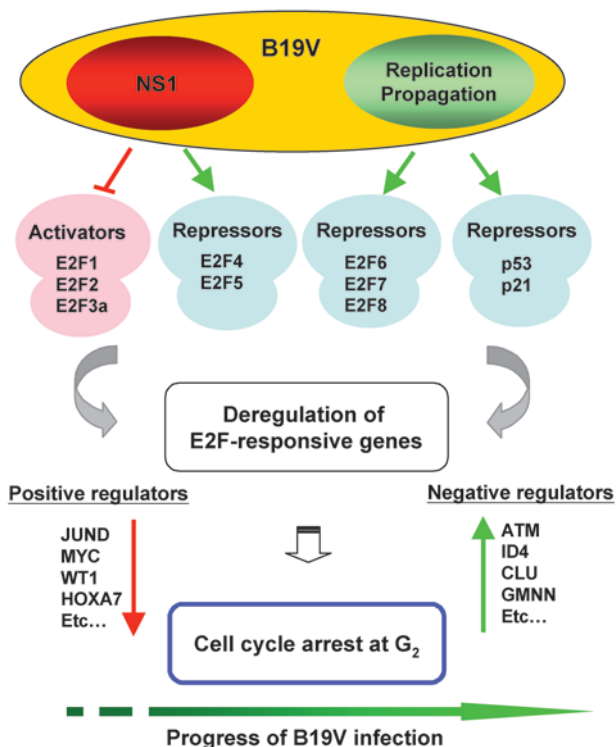
Figure 10
Schematic model of B19V NS1-mediated stable G₂ arrest and its biological consequences in erythroid progenitors. In early-stage B19V infection, association of NS1 with E2F4 or E2F5 enhances nuclear import of these repressive E2Fs, leading to stable G₂ arrest. Concomitantly, downregulation of E2F target genes eventually impairs the erythroid differentiation. Viral DNA replication and RNA transcription are enhanced by activation of G₂-related transcription factors and/or DNA repair proteins, causing activation of the p53 signal transduction and upregulation of E2F7 and E2F8, as part of the DNA damage response, which in turn blocks cell cycle progression.

using helper plasmids (pCAG-VSVG, pCAG-HIV-gp, and pCAG4-RTR2; gifts from A. Nienhuis) as previously described (61). NS1 or control lentivirus was transduced to CD36⁺ EPCs at an MOI of 4, unless otherwise stated.

For construction of a lentiviral plasmid carrying NS1mt with a mutated NLS, we searched for a putative NLS in the B19V NS1 protein using a Web-based program (PSORT WWW Server; <http://psort.hgc.jp/>) and found a cluster of basic amino acid residues (KKRP) between amino acids 177 and 180 that was homologous to the consensus sequence of eukaryotic NLS. A substitution mutation of K177C was introduced into the wild-type NS1 gene in pCMV-FlagNS1 by site-directed mutagenesis using the QuikChange Site-Directed Mutagenesis kit (Stratagene). The mutated NS1 gene was PCR-amplified and cloned between *EcoRI* and *NotI* sites in pCL20c MSCV-GFP, resulting in a recombinant lentiviral plasmid, pCL20c MSCV-NS1-NLS(K177C). NS1mt lentivirus was produced using pCL20c MSCV-NS1-NLS(K177C) (61) and transduced to CD36⁺ EPCs at an MOI of 4.

Recombinant lentiviruses carrying various siRNAs were produced as described previously (61), using the following lentiviral plasmids purchased from Open Biosystems: pGIPZ-E2F4 siRNA (target sequence: AGCGGATT-TACGACATTACCAA), pGIPZ-E2F5 siRNA (target sequence: GACTCAT-TACTTGTCTTAT), pGIPZ-nonsilencing (target sequence: ATCTCGCTT-GGGCGAGAGTAAG), and pGIPZ-GAPDH siRNA (target sequence: CCCTCATTTCCTGGTATGACAA). To assess the effects of E2F4 siRNA and E2F5 siRNA on NS1-induced G₂ arrest, we first transduced CD36⁺ EPCs with siRNA lentivirus (E2F4 siRNA, E2F5 siRNA, nonsilencing siRNA, or GAPDH siRNA) at an MOI of 20, according to the manufacturer's instruction. After 24 hours, cells were transduced with NS1 or control lentivirus at an MOI of 4 and harvested at 24 and 48 hpi for subsequent analyses.

Immunoblot, immunoprecipitation, and immunofluorescence analyses. Whole cell lysates were prepared using M-PRE Mammalian Protein Extraction Reagent (Pierce) supplemented with Complete Protease Inhibitor Cocktail (Roche) and Phosphatase Inhibitor Cocktail 2 (Sigma-Aldrich). After removal of cell debris by centrifugation, whole cell lysates were subjected to SDS-PAGE (4%–12%) and then transferred to a nitrocellulose membrane.





After blocking, the membrane was incubated with primary antibody at 4°C overnight and then secondary antibody at room temperature for 2 hours, followed by incubation with SuperSignal Chemiluminescent Reagent (Pierce) and then exposure to X-ray film.

For immunoprecipitation, 2×10^6 cells were lysed in 500 μ l high-salt lysis buffer (300 mM NaCl, 1 mM EDTA, 0.1% SDS, 1% Triton X-100, 0.1% sodium deoxycholate, and 20 mM Tris-HCl, pH 8.0). After preclearing with Protein G Sepharose (GE Healthcare), whole cell lysates were incubated with 4 μ g of respective antibodies overnight at 4°C, followed by additional 1-hour incubation at 4°C by addition of Protein G Sepharose. After washing with lysis buffer, samples were resuspended in 2 \times Laemmli buffer, boiled for 5 minutes, and subjected to SDS-PAGE (4%–12%) and then immunoblot analysis.

For IF analysis, cells were cytocentrifuged (Shandon Cytospin) and fixed in a methanol-acetone (1:1, v/v) solution. For double staining, cells were incubated with each primary antibody (1:200 dilution) in 10% FBS/0.02% Tween-20/PBS for 1 hour at 37°C and then secondary antibody (1:200 dilution) conjugated to either FITC or Alexa Fluor 568 (Invitrogen). After washing with PBS, cells were covered with mounting medium containing DAPI (Vectashield; Vector Laboratories) and subsequently examined by confocal microscopy using a Zeiss LSM 510 microscope. Fluorescence images were captured sequentially, using a 360-nm or 405-nm laser line and emission 385–470 nm for DAPI; a 488-nm laser line and emission between 505 and 550 nm for FITC; and a 561-nm laser line and emission between 575 and 615 nm for Alexa Fluor 568 using a 63 \times NA1.4 oil-immersion objective under conditions avoiding bleed-through. In addition to single optical sections, whole cell staining was evaluated on series of images taken along a z axis. These series were deconvolved using Huygens software (Scientific Volume Imaging), prior to 3D reconstruction and colocalization analyses both performed with Imaris software (Bitplane). Quantification of colocalization was assessed, and pixel codistribution was calculated for green and red staining patterns throughout the 3D data sets. Colocalized pixels (voxels in 3D) were displayed in a white mask overlapping the fluorescence channels over the image and also as a 2-color histogram (scattergram-fluorogram). To assess changes in distribution over cytoplasm and nucleus, the intensity line profile feature of Zeiss software was used: confocal images were analyzed by drawing an intensity line profile of cells in transverse section, and fluorescence intensities of each channel were plotted as histograms. Images were assembled using Photoshop software (Adobe).

The following antibodies were used in immunoblot, immunoprecipitation, and IF analyses: antibodies to E2F1 (sc-193), E2F3 (sc-879), E2F4 (sc-866), E2F4 (sc-56667), E2F6 (sc-53273), p53 (sc-126), p53 phospho-Ser20 (sc-18079-R), p21 (sc-871), GAPDH (sc-47724), and β -actin (sc-8432) (Santa Cruz Biotechnology Inc.); antibodies to E2F2 (ab65222), E2F5 (ab59769), E2F8 (ab57775), and p53 phospho-Ser15 (ab1431) (Abcam); anti-Flag M2 antibody (F1804, Sigma-Aldrich); HRP-rabbit anti-mouse IgG (61-6520, Invitrogen); HRP-anti-rabbit antibody (AL13404, Camarillo).

Cell proliferation, cell cycle, and apoptosis analyses. Cell proliferation was monitored using the Nexcelom Cellometer Auto T4 (Isogen Life Science) in triplicate. Cellular genomic DNA synthesis, cell cycle, and apoptosis were analyzed using the APC BrdU Flow kit (BD Biosciences – Pharmingen), the NUCYCL PI kit (Exalpha Biologicals), and the FITC Annexin V Apoptosis Detection Kit I (BD Biosciences – Pharmingen), respectively, according to manufacturers' instructions.

Microarray data processing and analysis. For transcriptional profiling induced by B19V NS1, CD36⁺ EPCs were transduced with NS1 or control lentivirus in

triplicate at an MOI of 4 and collected at 12, 24, and 48 hpt. Total RNA was isolated and purified using the RNeasy Micro kit (QIAGEN), according to the manufacturer's instructions. Quality and integrity of RNA were assessed by the Agilent 2100 Bioanalyzer (Agilent Technologies). T7-based RNA amplification was carried out using total RNA (1 μ g) as suggested by the manufacturer. In vitro transcription and biotin labeling of purified cDNA were performed with T7 RNA polymerase using the Affymetrix IVT labeling kit. Biotin-labeled RNA (20 μ g) was fragmented and hybridized to Affymetrix HG-U133 Plus 2 arrays.

Affymetrix GeneChip operating software (version 1.4) was used to calculate the MASS signal intensity values for the 54,675 probe sets on Affymetrix HG-U133 Plus 2 arrays and to estimate presence/absence for each of the probe sets in signal intensity on the arrays. The signal intensity values were subsequently transformed with an adaptive variance-stabilizing, quantile-normalizing transformation (The Mathematical and Statistical Computing Lab Analyst's Toolbox can be freely downloaded from <http://abs.cit.nih.gov/MSCLtoolbox/>). Transformation data from all the arrays were subjected to principal component analysis to detect outliers. Six-level 1-way ANOVA analysis was performed to evaluate any differences among 6 groups (NS1 and control at 12, 24, and 48 hpt) in probe sets. Probe sets/genes with an FDR of 10% or less using the Benjamini-Hochberg procedure (1.5-fold change between NS1 and control at any of 12, 24, and 48 hpt) and present calls were selected. JMP statistical software package 7.0 (SAS Institute) was used in microarray data analysis. Hierarchical clustering analysis was used. The selected probe sets/genes were further analyzed for main pathways and biological functions with Ingenuity software (Ingenuity Systems). The primary CEL files have been deposited in the public repository Gene Expression Omnibus (GEO); <http://www.ncbi.nlm.nih.gov/geo/>, with accession number GSE18906.

Real-time PCR and real-time RT-PCR. To quantitatively evaluate B19V infection, we performed real-time PCR as described previously (36). To confirm changes in putative E2F4 target genes induced by B19V NS1, we performed SYBR green-based real-time PCR using the RT² qPCR Primer Assay kit (SuperArray Bioscience) following the manufacturer's instructions. Data were analyzed using the comparative cycle threshold method $\Delta\Delta C(t)$ with normalization of the raw data to housekeeping genes (*HPRT1*, *RPL13A*, *GAPDH*, and *ACTB*).

Real-time RT-PCR was conducted with adequate primers and probes targeting the *B19V NS1* gene, which was amplified as a multiplex with β -actin as an internal control. Each amplicon was quantitated by interpolation with the respective standard curve to each target (*NS1* or *ACTB*) constructed with serial dilutions of the corresponding plasmid.

Statistics. Data are expressed as mean \pm SD. Statistical significance was determined by a 2-tailed Student's *t* test, with a *P* value less than 0.05 considered statistically significant.

Acknowledgments

This work was supported by the NIH Intramural Research Program. We thank Dong Joo Kim for help in preparing the manuscript.

Received for publication November 19, 2009, and accepted in revised form August 4, 2010.

Address correspondence to: Ning Zhi, Hematology Branch, National Heart, Lung, and Blood Institute, NIH, Bldg 10CRC/Rm 3E-5272, 9000 Rockville Pike, Bethesda, Maryland 20892-1652, USA. Phone: 301.451.7137; Fax: 301.496.8396; E-mail: zhin@nhlbi.nih.gov.

1. Young NS, Brown KE. Parvovirus B19. *N Engl J Med*. 2004;350(6):586–597.
2. Matsumura M. Parvovirus-associated arthritis. *Am J Med*. 2001;111(3):241.
3. Moore TL. Parvovirus-associated arthritis. *Curr Opin Rheumatol*. 2000;12(4):289–294.
4. Alvarez-Lafuente R, et al. Human parvovirus B19,

- varicella zoster virus, and human herpes virus 6 in temporal artery biopsy specimens of patients with giant cell arteritis: analysis with quantitative real time polymerase chain reaction. *Ann Rheum Dis*. 2005;64(5):780–782.
5. Scheurle W, Ramasubbu K, Wachowski O, Hemauer AF, Modrow S. Chronic autoimmune

thrombopenia/neutropenia in a boy with persistent parvovirus B19 infection. *J Clin Virol*. 2001; 20(3):173–178.

6. Weigel-Kelley KA, Yoder MC, Srivastava A. Alpha-5beta1 integrin as a cellular coreceptor for human parvovirus B19: requirement of functional activation of beta1 integrin for viral entry. *Blood*.



2003;102(12):3927–3933.

7. Brown KE, Anderson SM, Young NS. Erythrocyte P antigen: cellular receptor for B19 parvovirus. *Science*. 1993;262(5130):114–117.

8. Guan W, et al. Block to the production of full-length B19 virus transcripts by internal polyadenylation is overcome by replication of the viral genome. *J Virol*. 2008;82(20):9951–9963.

9. Liu JM, Green SW, Shimada T, Young NS. A block in full-length transcript maturation in cells nonpermissive for B19 parvovirus. *J Virol*. 1992;66(8):4686–4692.

10. Agbandje M, Kajigaya S, McKenna R, Young NS, Rossmann MG. The structure of human parvovirus B19 at 8 Å resolution. *Virology*. 1994;203(1):106–115.

11. Zadori Z, et al. A viral phospholipase A2 is required for parvovirus infectivity. *Dev Cell*. 2001;1(2):291–302.

12. Dorsch S, et al. The VP1 unique region of parvovirus B19 and its constituent phospholipase A2-like activity. *J Virol*. 2002;76(4):2014–2018.

13. Filippone C, et al. VP1u phospholipase activity is critical for infectivity of full-length parvovirus B19 genomic clones. *Virology*. 2008;374(2):444–452.

14. Chen AY, et al. The small 11 kDa nonstructural protein of human parvovirus B19 plays a key role in inducing apoptosis during B19 virus infection of primary erythroid progenitor cells. *Blood*. 2010;115(5):1070–1080.

15. Zhi N, Mills IP, Lu J, Wong S, Filippone C, Brown KE. Molecular and functional analyses of a human parvovirus B19 infectious clone demonstrates essential roles for NS1, VP1, and the 11-kilodalton protein in virus replication and infectivity. *J Virol*. 2006;80(12):5941–5950.

16. Raab U, Beckenlehner K, Lowin T, Niller HH, Doyle S, Modrow S. NS1 protein of parvovirus B19 interacts directly with DNA sequences of the p6 promoter and with the cellular transcription factors Sp1/Sp3. *Virology*. 2002;293(1):86–93.

17. Gareus R, et al. Characterization of cis-acting and NS1 protein-responsive elements in the p6 promoter of parvovirus B19. *J Virol*. 1998;72(1):609–616.

18. Morita E, et al. Human parvovirus B19 induces cell cycle arrest at G(2) phase with accumulation of mitotic cyclins. *J Virol*. 2001;75(16):7555–7563.

19. Morita E, Nakashima A, Asao H, Sato H, Sugamura K. Human parvovirus B19 nonstructural protein (NS1) induces cell cycle arrest at G(1) phase. *J Virol*. 2003;77(5):2915–2921.

20. Sol N, et al. Possible interactions between the NS-1 protein and tumor necrosis factor alpha pathways in erythroid cell apoptosis induced by human parvovirus B19. *J Virol*. 1999;73(10):8762–8770.

21. Fu Y, Ishii KK, Munakata Y, Saitoh T, Kaku M, Sasaki T. Regulation of tumor necrosis factor alpha promoter by human parvovirus B19 NS1 through activation of AP-1 and AP-2. *J Virol*. 2002;76(11):5395–5403.

22. Nakashima A, Morita E, Saito S, Sugamura K. Human Parvovirus B19 nonstructural protein transactivates the p21/WAF1 through Sp1. *Virology*. 2004;329(2):493–504.

23. Momoeda M, Wong S, Kawase M, Young NS, Kajigaya S. A putative nucleoside triphosphate-binding domain in the nonstructural protein of B19 parvovirus is required for cytotoxicity. *J Virol*. 1994;68(12):8443–8446.

24. Dimova DK, Dyson NJ. The E2F transcriptional network: old acquaintances with new faces. *Oncogene*. 2005;24(17):2810–2826.

25. Stevaux O, Dyson NJ. A revised picture of the E2F transcriptional network and RB function. *Curr Opin Cell Biol*. 2002;14(6):684–691.

26. Crosby ME, Jacobberger J, Gupta D, Macklis RM, Almasan A. E2F4 regulates a stable G2 arrest response to genotoxic stress in prostate carcinoma. *Oncogene*. 2007;26(13):1897–1909.

27. Gaubatz S, et al. E2F4 and E2F5 play an essential role in pocket protein-mediated G1 control. *Mol Cell*. 2000;6(3):729–735.

28. Ren B, et al. E2F integrates cell cycle progression with DNA repair, replication, and G(2)/M checkpoints. *Genes Dev*. 2002;16(2):245–256.

29. Farkas T, Hansen K, Holm K, Lukas J, Bartek J. Distinct phosphorylation events regulate p130- and p107-mediated repression of E2F-4. *J Biol Chem*. 2002;277(30):26741–26752.

30. Calbo J, et al. G1 cyclin/cyclin-dependent kinase-coordinated phosphorylation of endogenous pocket proteins differentially regulates their interactions with E2F4 and E2F1 and gene expression. *J Biol Chem*. 2002;277(52):50263–50274.

31. Olgiate J, Ehmann GL, Vidyarthi S, Hilton MJ, Bachheimer SL. Herpes simplex virus induces intracellular redistribution of E2F4 and accumulation of E2F pocket protein complexes. *Virology*. 1999;258(2):257–270.

32. Ohtani N, et al. Epstein-Barr virus LMP1 blocks p16INK4a-RB pathway by promoting nuclear export of E2F4/5. *J Cell Biol*. 2003;162(2):173–183.

33. Laughlin-Drubin ME, Munger K. The human papillomavirus E7 oncoprotein. *Virology*. 2009;384(2):335–344.

34. Schaley JE, Polonskaia M, Hearing P. The adenovirus E4-6/7 protein directs nuclear localization of E2F-4 via an arginine-rich motif. *J Virol*. 2005;79(4):2301–2308.

35. Batchu RB, Shammam MA, Wang JY, Munshi NC. Dual level inhibition of E2F-1 activity by adeno-associated virus Rep78. *J Biol Chem*. 2001;276(26):24315–24322.

36. Wong S, et al. Ex vivo-generated CD36+ erythroid progenitors are highly permissive to human parvovirus B19 replication. *J Virol*. 2008;82(5):2470–2476.

37. Amati B, Alevizopoulos K, Vlach J. Myc and the cell cycle. *Front Biosci*. 1998;3:d250–d268.

38. Yamagami T, et al. Suppression of Wilms' tumor gene (WT1) expression induces G2/M arrest in leukemic cells. *Leuk Res*. 1998;22(4):383–384.

39. Becker TM, et al. The chromatin remodelling factor BRG1 is a novel binding partner of the tumor suppressor p16INK4a. *Mol Cancer*. 2009;8:4.

40. Mishra BP, Ansari KI, Mandal SS. Dynamic association of MLL1, H3K4 trimethylation with chromatin and Hox gene expression during the cell cycle. *FEBS J*. 2009;276(6):1629–1640.

41. Simmen RC, Zhang XL, Michel FJ, Min SH, Zhao G, Simmen FA. Molecular markers of endometrial epithelial cell mitogenesis mediated by the Sp/Kruppel-like factor BTEB1. *DNA Cell Biol*. 2002;21(2):115–128.

42. Kuntzen C, et al. Inhibition of c-Jun-N-terminal-kinase sensitizes tumor cells to CD95-induced apoptosis and induces G2/M cell cycle arrest. *Cancer Res*. 2005;65(15):6780–6788.

43. Bakiri L, Matsuo K, Wisniewska M, Wagner EF, Yaniv M. Promoter specificity and biological activity of tethered AP-1 dimers. *Mol Cell Biol*. 2002;22(13):4952–4964.

44. Lahlil R, Lecuyer E, Herblot S, Hoang T. SCL assembles a multifactorial complex that determines glycophorin A expression. *Mol Cell Biol*. 2004;24(4):1439–1452.

45. Brand M, et al. Dynamic changes in transcription factor complexes during erythroid differentiation revealed by quantitative proteomics. *Nat Struct Mol Biol*. 2004;11(1):73–80.

46. Vodyanik MA, Thomson JA, Slukvin II. Leukosialin (CD43) defines hematopoietic progenitors in human embryonic stem cell differentiation cultures. *Blood*. 2006;108(6):2095–2105.

47. Carter JH, Lefebvre JM, Wiest DL, Tourtellotte WG. Redundant role for early growth response transcriptional regulators in thymocyte differentiation and survival. *J Immunol*. 2007;178(11):6796–6805.

48. Davy C, Doorbar J. G2/M cell cycle arrest in the life cycle of viruses. *Virology*. 2007;368(2):219–226.

49. Wahl AF, et al. Loss of normal p53 function confers sensitization to Taxol by increasing G2/M arrest and apoptosis. *Nat Med*. 1996;2(1):72–79.

50. Zimmerman ES, et al. Human immunodeficiency virus type 1 Vpr induces DNA replication stress in vitro and in vivo. *J Virol*. 2006;80(21):10407–10418.

51. Gaubatz S, Lees JA, Lindeman GJ, Livingston DM. E2F4 is exported from the nucleus in a CRM1-dependent manner. *Mol Cell Biol*. 2001;21(4):1384–1392.

52. Moberg K, Starz MA, Lees JA. E2F-4 switches from p130 to p107 and pRB in response to cell cycle reentry. *Mol Cell Biol*. 1996;16(4):1436–1449.

53. Hateboer G, Kerkhoven RM, Shvarts A, Bernards R, Beijersbergen RL. Degradation of E2F by the ubiquitin-proteasome pathway: regulation by retinoblastoma family proteins and adenovirus transforming proteins. *Genes Dev*. 1996;10(23):2960–2970.

54. Koury MJ, Sawyer ST, Brandt SJ. New insights into erythropoiesis. *Curr Opin Hematol*. 2002;9(2):93–100.

55. Munugalavada V, Kapur R. Role of c-Kit and erythropoietin receptor in erythropoiesis. *Crit Rev Oncol Hematol*. 2005;54(1):63–75.

56. Lilley CE, Schwartz RA, Weitzman MD. Using or abusing: viruses and the cellular DNA damage response. *Trends Microbiol*. 2007;15(3):119–126.

57. Zalmas LP, et al. DNA-damage response control of E2F7 and E2F8. *EMBO Rep*. 2008;9(3):252–259.

58. Banin S, et al. Enhanced phosphorylation of p53 by ATM in response to DNA damage. *Science*. 1998;281(5383):1674–1677.

59. Shimomura S, Wong S, Brown KE, Komatsu N, Kajigaya S, Young NS. Early and late gene expression in UT-7 cells infected with B19 parvovirus. *Virology*. 1993;194(1):149–156.

60. Zhi N, Zadori Z, Brown KE, Tijssen P. Construction and sequencing of an infectious clone of the human parvovirus B19. *Virology*. 2004;318(1):142–152.

61. Persons DA, Hargrove PW, Allay ER, Hanawa H, Nienhuis AW. The degree of phenotypic correction of murine beta-thalassemia intermedia following lentiviral-mediated transfer of a human gamma-globin gene is influenced by chromosomal position effects and vector copy number. *Blood*. 2003;101(6):2175–2183.